University Library

MINERVA ACCESS

A gateway to Melbourne's research publications

Minerva Access is the Institutional Repository of The University of Melbourne

Author/s:
Hu, G;Xiao, G;Guo, Y;Manning, M;Chen, L;Yu, L;Li, KG;May, EF

Title:
Separation of methane and nitrogen using ionic liquidic zeolites by pressure vacuum swing adsorption

Date:
2022-07-01

Citation:
Hu, G., Xiao, G., Guo, Y., Manning, M., Chen, L., Yu, L., Li, K. G. & May, E. F. (2022). Separation of methane and nitrogen using ionic liquidic zeolites by pressure vacuum swing adsorption. Aiche Journal, 68 (7), https://doi.org/10.1002/aic.17668.

Persistent Link:
https://hdl.handle.net/11343/308140

License:
CC BY-NC

Check for updates

Received: 26 October 2021 | Revised: 17 January 2022 | Accepted: 17 February 2022

DOI: 10.1002/aic.17668

AIChE JOURNAL

RESEARCH ARTICLE

Separations: Materials, Devices and Processes

Separation of methane and nitrogen using ionic liquidic zeolites by pressure vacuum swing adsorption

Guoping Hu[1,2] | Gongkui Xiao[1] | Yalou Guo[2] | Mitch Manning[3] | Li Chen[4] | Lanjin Yu[4] | Kevin Gang Li[2] | Eric F. May[1]

[1]Fluid Science & Resources Division, Department of Chemical Engineering, The University of Western Australia, Crawley, Western Australia, Australia

[2]Department of Chemical Engineering, The University of Melbourne, Parkville, Victoria, Australia

[3]Gas Capture Technologies Pty., Ltd, Cockburn, Western Australia, Australia

[4]DKT Energy Technology Co., Ltd, Chengdu, Sichuan, China

Correspondence
Kevin Gang Li, Department of Chemical Engineering, The University of Melbourne, Victoria 3010, Australia.
Email: li.g@unimelb.edu.au
Eric F. May, The University of Western Australia, 35 Stirling Highway, Perth, Western Australia 6009, Australia.
Email: eric.may@uwa.edu.au

Funding information
Australian Research Council, Grant/Award Number: DP190100983; Department of Industry, Innovation and Science, Australian Government; University of Melbourne

Abstract

The separation of methane (CH_4) and nitrogen (N_2) is a significant challenge to the enrichment and utilization of low concentration CH_4 due to the similarity in the physical and chemical properties of the two molecules. In this work, we investigated the separation of CH_4 from N_2 using 100 kg of a new ionic liquidic zeolite (ILZ) material in a 6-bed pilot-scale pressure swing adsorption process. Feed gases with CH_4 concentrations of 5.0% and 16.1% were upgraded to 11.5% and 34.6%, respectively, with CH_4 recoveries higher than 80%. The pilot test results were used to anchor a numerical model that then allowed the efficient investigation of multiple operational parameters including desorption pressure and feed gas flow rates. The numerical model produced CH_4 concentrations for both product streams consistent with those measured in the pilot experiments, with root mean square deviations below 2%. The modeling results revealed that sufficiently low desorption pressures can unexpectedly lead to lower heavy product purities under limited feed gas flow conditions. Furthermore, the optimum feed gas flow rate under which maximum heavy product purity is achieved increases with lower desorption pressure. The maximum CH_4 concentrations increased from 31.8% to 41.5%, as desorption pressures decreased from 22.8 to 12.2 kPa for optimum feed flow rates between 78.2 and 105.5 mol/h. We also demonstrate a method of process optimization based on the bed capacity ratio, $\mathbb{C}$, which provides a scale-independent measure of the degree to which the column is being used effectively. By varying feed flow rate and/or desorption pressure, $\mathbb{C}$ values between 0.2 and 0.8 were explored, with maxima in the combined separation performance metric (methane recovery) $\times$ (methane purity) occurring for values of $\mathbb{C}$ in the range 0.29–0.36. This separation performance optimization by adjusting $\mathbb{C}$ provides an effective strategy for integrating and understanding the impact of multiple operating parameters.

KEYWORDS
adsorbent, ILZ, methane, pressure swing adsorption, separation

This is an open access article under the terms of the Creative Commons Attribution-NonCommercial License, which permits use, distribution and reproduction in any medium, provided the original work is properly cited and is not used for commercial purposes.
© 2022 The Authors. *AIChE Journal* published by Wiley Periodicals LLC on behalf of American Institute of Chemical Engineers.

1 | INTRODUCTION

Methane (CH_4) is an important energy carrier with the lowest carbon intensity among fossil fuels. More importantly for those with limited access to energy, for the same power output, the combustion of methane produces less than half the CO_2 compared with coal, and nearly no particulate matter. Methane is also the second largest anthropological greenhouse gas[1] and is emitted principally by the natural gas industry, coal mining operations and agriculture.[2–5] Therefore, the capture of CH_4 from these sources is essential to global initiatives aimed at reducing greenhouse gas emissions. Additionally, methane capture has the potential to provide a source of useful low-cost energy and deliver significant social benefits[6] with comparatively few emissions if it can be recovered and purified at sufficiently low cost. However, nitrogen (N_2) is a key impurity often present in low grade sources of natural gas, and the separation of N_2/CH_4 represents a significant challenge to the efficient upgrade of methane from such sources due to the similarities in the volatility, kinetic diameter, dipole moment, and polarizability of these two molecules.[7]

The need for N_2/CH_4 separations occurs in a wide variety of industrial applications such as natural gas processing, coal seam gas (CSG) upgrading, landfill gas production and biogas enrichment. The gas compositions in these applications vary significantly depending on the gas source produced by the application. Nitrogen rejection can be used in the treatment of boil off gas (BOG) generated by liquefied natural gas (LNG) production, where the initial N_2 concentration can range from 7% to 22% with balance being CH_4.[8,9] Methane upgrading of biogases, which usually includes both CO_2 removal[10] and N_2 rejection,[11] mainly focuses on feed nitrogen concentrations between 0% and 33%.[12,13] CSG is another major methane source, and with gas compositions varying substantially from 0.5% to 99% CH_4. However, for two thirds of coal mines emitting gas, the methane concentration is below 25%, balanced with nitrogen or air.[14]

A range of chemical separation technologies have been explored to overcome the N_2/CH_4 separation challenge such as solvent absorption,[15] adsorption,[16–18] membrane separation,[19] and cryogenics.[20] Among these technologies, adsorption has been widely used to process gas flows at scales from 10 to 100,000 $Sm^3 \cdot h^{-1}$ (20°C and 1.01 bar), using pressure-vacuum swing adsorption (PVSA) processes with various adsorbents such as carbon molecular sieve (CMS),[21,22] Engelhard titanosilicate type 4 (ETS-4)[23,24] and activated carbon.[25,26] The separation of CH_4/N_2 using CMS is often achieved by exploiting differences in adsorption kinetics,[27] while ETS-4 is a N_2 selective adsorbent that can be favorably applied to treat in gas sources with low N_2 concentrations.[24] Activated carbon is the cheapest adsorbent and has high CH_4 uptake (approximately 1 mol CH_4/kg at 1 bar and 25°C); however, its separation performance is limited by the a relatively modest CH_4/N_2 selectivity (around 3–4 at equimolar concentrations, 25–30°C, and pressures of 1–10 bar).[17,26]

Li et al.[28] developed a new porous material, named ionic liquidic zeolite (ILZ), which has relatively high CH_4/N_2 selectivity (6–8 at equimolar concentrations and pressure of 1–10 bar) and moderate CH_4 adsorption capacity (approximately 0.5 mol/kg at 1 bar and 25°C). The performance of this material in separating various feeds of CH_4/N_2 mixtures has been explored in the context of dual-reflux pressure swing adsorption (DR-PSA) processes via both numerical modeling and laboratory-scale experiments.[28–31] The results presented clearly show that, when used in the same process to treat the same feed gas, ILZ had a better N_2/CH_4 separation performance than either activated carbon or ETS-4, achieving both higher CH_4 purity and recovery. Analysis of the associated process duties also showed that the use of ILZ required 11% less energy per cycle than activated carbon. However, these analyses were mainly on laboratory scale experiments and corresponding process simulations, and the performance of ILZ when applied in an industrial separation process still required empirical demonstration.

The primary target of this research is to better understand the capture and upgrade of methane from low grade CSG sources containing 5%–15% CH_4 balanced with N_2 and to establish a robust numerical model for process optimization. In this work, we tested the performance of 112 kg of ILZ for the separation of CH_4 and N_2 using a commercial pilot scale PVSA facility consisting of six columns. The PVSA system allows three pressure equalization steps and delivers a continuous product flow with the ability to maximize CH_4 recovery and concentration. To investigate cycle parameter sensitivities, we also established a robust numerical model using the Aspen Adsorption software platform, which revealed some unexpected insights and enabled further process optimization. The objective of this article is to convey these insights: the numerical simulations reported are anchored and validated by the pilot-scale results but necessarily go far beyond them in order to understand the experimental outcomes and guide the design of future PSA cycles.

2 | METHODS

2.1 | Pilot plant tests

The pilot experiments were conducted using a 6-column PVSA facility, the details of which been described in our previous work, so only a brief summary is given here.[32] The dimensions of the adsorption columns and the packing details of adsorbents are provided in Table 2. The 6-column system allows continuous flow of the feed gas, light, and heavy products to ensure stable operation. The packed volume of the PVSA facility is 210 L with each column having a volume of 35 L. Each column is packed with three layers of adsorbents: a guard layer of alumina (approximately 0.19 m) at the bottom of the column to remove any moisture; a protection layer of activated carbon (0.27 m) to remove any heavy hydrocarbons; and an adsorption layer of ILZ for the separation of CH_4 and N_2. This layout is commonly employed to separate different components, protect the adsorbent layer, extend the life span of adsorbents while maintaining similar separation performance. The methane concentrations of the feed (c_{fed}), light (c_{light}), and heavy (c_{heavy}) streams were measured using infrared gas analysers (QGS-084, 0%–100%, ±1 mol% full scale). The recovery (R) and productivity (Y) of CH_4 are calculated using Equations (1) and (2),

TABLE 1 The step sequence of the PVSA process

Step	1	2	3	4	5	6	7	8	9	10	11	12
Description	Ads	Ads	PE1↓	PE2↓	PE3↓	Idle	Des	Des	PE3↑	PE2↑	PE1↑	Rep

Note: PE↑ denotes pressure increasing via the pressure equalization step, PE↓ denotes pressure decreasing through the pressure equalization step.

TABLE 2 The details of adsorption columns and model parameters

Parameter			Unit	Values		
Column height			m	2.0		
Column diameter			m	0.15		
Column number			–	6		
Column wall thickness			m	0.005		
Wall specific heat capacity			J/g/K	0.5		
Wall thermal conductivity			W/m/K	45		
Wall density			kg/m^3	7850		
Parameter				ILZ	Activated carbon	Alumina
Adsorbent diameter			m	0.00205	0.004	0.0035
Inter-particle voidage			m^3/m^3	0.340	0.550	0.325
Intra-particle voidage			m^3/m^3	0.356	0.370	0.693
Bulk density			kg/m^3	700	540	800
Adsorbent specific heat capacity			J/g/K	1.50	1.00	0.45
Heat of adsorption (CH_4)			kJ/mol	−20.24	−20.09	−19.05
Heat of adsorption (N_2)			kJ/mol	−16.61	−17.84	−24.61
Layer height			m	1.52	0.28	0.19
Heat transfer coefficient between gas and wall (both sides)			W/m^2/K	10	10	10
Mass transfer coefficient	CH_4		s^{-1}	1	1	1
	N_2		s^{-1}	5	3	5
Isotherm parameter	CH_4	Q_{max}	mmol/g	3.02	2.87	1.03
		B	10^{-6}, 1/kPa	0.54	1.94	0.19
		ΔH	kJ/mol	20.24	20.09	19.04
	N_2	Q_{max}	mmol/g	1.96	1.97	1.54
		B	10^{-6}, 1/kPa	0.77	1.52	0.0038
		ΔH	kJ/mol	16.61	17.84	24.61

respectively, where F_{fed} denotes the flow rate of feed gas, and m is the total mass of adsorbents.

$$R = \frac{c_{heavy}\left(c_{fed} - c_{light}\right)}{c_{fed}\left(c_{heavy} - c_{light}\right)} \times 100, \quad (1)$$

$$Y = \frac{F_{fed} \cdot R}{m}. \quad (2)$$

The ILZ adsorbent was obtained from Gas Capture Technologies (GCT) Pty. Ltd. and preferentially adsorbs methane over nitrogen via physisorption. Adsorption isotherms of nitrogen and methane on ILZ are provided in Figure S3. The ILZ consists of spherical beads, with white or light-yellow color and a diameter of 1.6–2.5 mm. It has high chemical and mechanical stability and an average particle compression strength of 30 N.

The PVSA process employed in this study consists of 12 steps including adsorption (Ads), pressure equalization (PE), desorption (Des), and repressurization (Rep). The objective of this cycle is to achieve a high CH_4 concentration in the heavy product and a high recovery of methane. The detailed sequence of the process is shown in Table 1 and Figure 1. In the Ads step, feed gas flows into the bottom of the column during which time methane is preferably adsorbed and a nitrogen rich exhaust (light product) is released from the top of the column. The column then undergoes three PE↓ steps, during which time gas in the void space transfers to other columns to increase methane purity and recovery and reduce the energy requirements of the cycle. Thereafter, the column is connected to a vacuum pump for desorption or adsorbent regeneration. The regenerated column is then connected to other columns for PE↑, which enables its pressure to increase. Last, the top of the column is connected to the light product tank for repressurization. This final step further raises

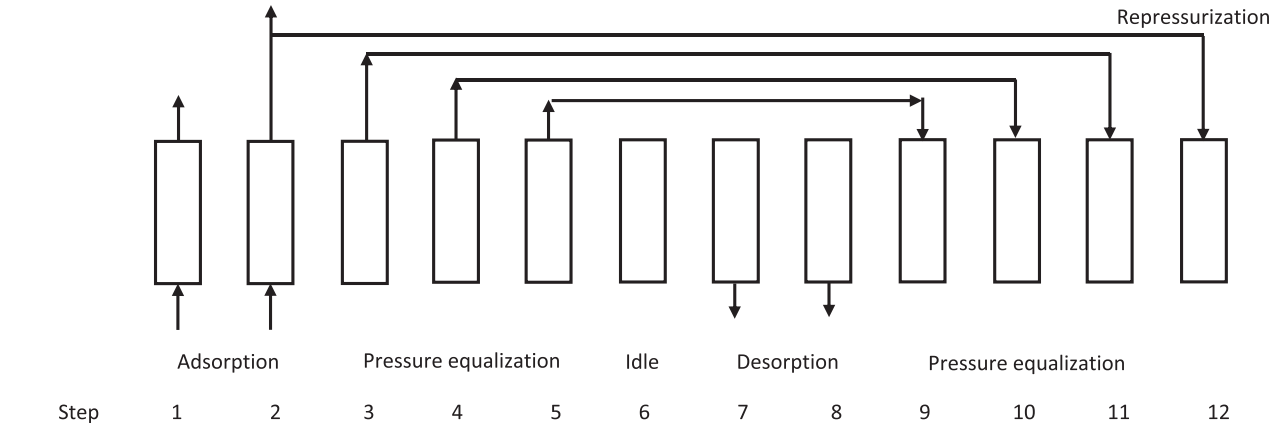

FIGURE 1 Schematic representation of the PVSA process

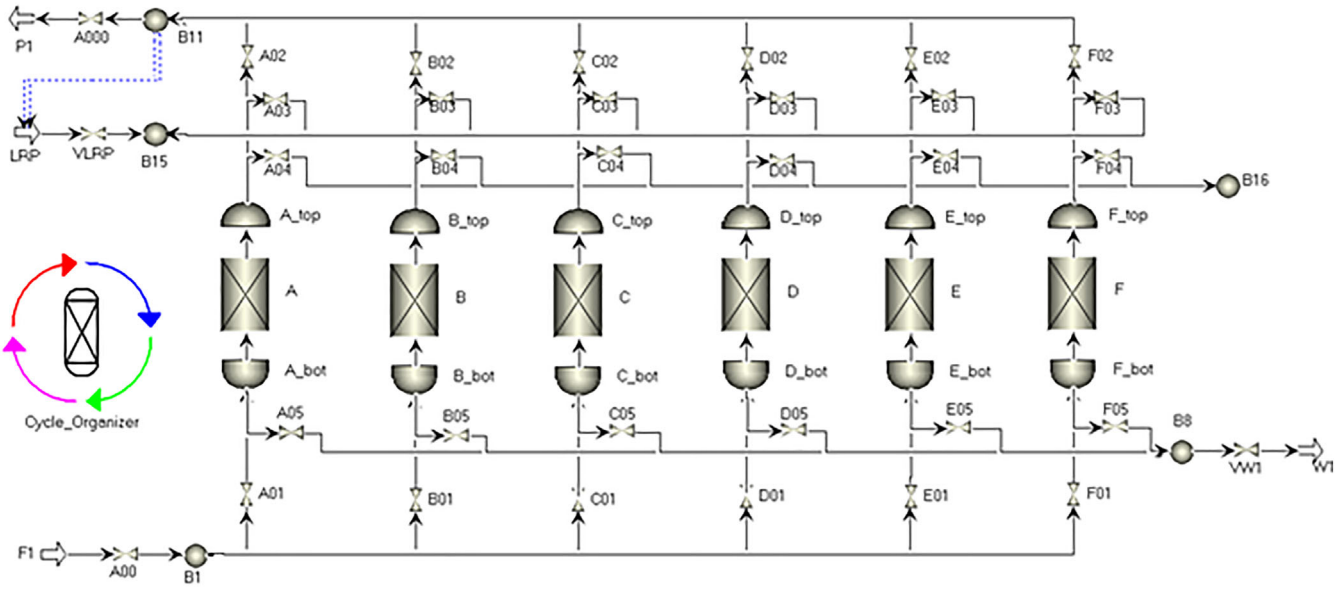

FIGURE 2 A snapshot of the 6-column PVSA model built in the Aspen Adsorption platform

the column pressure close to the feed gas pressure, which is crucial for avoiding the fluidization of the adsorbents. This step also improves methane recovery by moving the adsorption front downwards before any light product is produced from the top of the bed.

2.2 | Simulation

A 6-column PVSA process model was established (Figure 2) on the Aspen Adsorption platform to simulate the performance of the aforementioned pilot tests, and the dimensions of these columns (Table 2) are identical to the experimental facility (Section 2.1). The basic assumptions and governing equations used by the model are largely the same as those described by Zhang et al.[33] Only convectional gas flow was considered, and axial dispersion was neglected. The Ergun equation (Equation 3) was used to calculate the momentum balance,

$$\frac{\partial p}{\partial x} = -\left(\frac{150\times 10^{-5}\mu_g(1-\varepsilon_i)^2}{(2r_p\psi)^2\varepsilon_i^3}v_g + \frac{1.75\times 10^{-5}M_w\rho_g(1-\varepsilon_i)}{(2r_p\psi)\varepsilon_i^3}v_g^2\right), \quad (3)$$

where M_w is the molecular weight of gaseous mixture, P is the gas pressure, r_p is the particle radius, v_g is the superficial gas velocity, x is the axial distance coordinate, ε_i is the bed (interparticle) voidage, μ_g is the gas mixture viscosity, ρ_g is the gas density, ψ is the particle shape factor.

The kinetics were assumed to follow the lumped (linear) resistance model (Equation 4),

$$\frac{\partial w_i}{\partial t} = \mathrm{MTC}\left(w_i^* - w_i\right), \quad (4)$$

where w_i is the adsorbent loading of component i per unit mass of adsorbent, w_i^* is adsorbent loading of component i per unit mass of adsorbent in equilibrium with its partial pressure in gas phase, MTC is the mass transfer coefficient.

The adsorption isotherms were described using the Langmuir model (Equation 5).

$$Q = \frac{Q_{max} B p e^{\Delta H/RT}}{1 + B p e^{\Delta H/RT}}, \tag{5}$$

where Q is the adsorption capacity, Q_{max} is the saturated adsorption uptake, B is a constant, p is adsorption pressure, ΔH is the isosteric heat of adsorption, R is the gas constant, T is adsorption temperature.

Binary mixture adsorption isotherms were predicted using the extended Langmuir model (Equations 6 and 7),

$$Q_{CH_4} = \frac{Q_{max,CH_4} B_{CH_4} p_{CH_4} e^{\Delta H_{CH_4}/RT}}{1 + B_{CH_4} p_{CH_4} e^{\Delta H_{CH_4}/RT} + B_{N_2} p_{N_2} e^{\Delta H_{N_2}/RT}}, \tag{6}$$

$$Q_{N_2} = \frac{Q_{max,N_2} B_{N_2} p_{N_2} e^{\Delta H_{N_2}/RT}}{1 + B_{CH_4} p_{CH_4} e^{\Delta H_{CH_4}/RT} + B_{N_2} p_{N_2} e^{\Delta H_{N_2}/RT}}, \tag{7}$$

where Q is the adsorption capacity, Q_{max} is the saturated adsorption uptake, B is a constant, p is adsorption pressure, ΔH is the isosteric heat of adsorption, R is the gas constant, T is adsorption temperature.

No reactions were considered, and the energy balance was treated rigorously (i.e., non-isothermal). The heat transfer between the column and environment was estimated using a constant heat transfer coefficient and the axial thermal conduction was ignored for the gas and solid phases. The values for mass transfer coefficients (MTCs) were the same as those used by Weh et al.[29] and are based on the rapid adsorption kinetics reported by Li et al.[28] for the uptake of both CH_4 and N_2 on ILZ. Additionally, as demonstrated by Zhang et al.,[33] the results of such simulations are relatively insensitive to adsorption kinetics if the MTCs are equal to or greater than 1 s^{-1}. Numerical values for the key parameters used by the model are also listed in Table 2.

A cycle organizer is used to control the cyclic operation of this model, while the integration method used across the discretized bed was Implicit Euler.[33,34] The solution was considered to have converged when the maximum change in a variable was less than or equal to the specified absolute tolerance (10^{-5}) and the specified relative tolerance (10^{-5}) × variable value. The time step size was set as variable between 1 and 5 s to allow for both fast and high calculation accuracy. The partial differential equations of the model were solved using the finite difference method (FDM). The column was divided into 60 nodes for calculation. Gaussian elimination MA48 and mixed Newton method were used as the linear and nonlinear solvers, respectively. The Gaussian elimination MA48 solver features a good choice of pivot order, the ability to factorize a matrix with a given pivot order, and solution of the system of equations using the factorized matrix, while the Newton method is used for initialization and steady state steps and the Fast Newton method for dynamic steps.[33,34]

2.3 | Process and energy analysis

In practical PVSA systems, the time needed to achieve a target vacuum pressure (P_{target}) in the desorption step is often limited by the flow capacity of the vacuum pump (Figure S1). In our pilot plant, it took the vacuum pump 160 s to achieve P_{target} in each column, therefore, the time for the vacuum step in the simulations were specified as 160 s to match the experimental reality.

The primary objective of the CH_4/N_2 separations is to achieve simultaneously high CH_4 product purity, recovery while maximizing productivity and minimizing the energy consumption. As the demonstration experiments were conducted using an established PVSA pilot plant, the adsorption time was forced to be identical with the minimum desorption time (160 s) required by the vacuum pump to achieve the target vacuum pressure. Hence, optimization of the process was investigated under the constraint of fixed adsorption time while other operational parameters could be varied (i.e., feed concentration, desorption pressure and feed gas flow rate) to further explore and improve the CH_4/N_2 separation performance of this process.

The energy consumption of the vacuum pump (W) per mole of methane produced is estimated using Equation (8),[16]

$$W = \frac{\gamma RT}{\eta(\gamma - 1)} \left(\frac{P_{Dis}^{\frac{\gamma-1}{\gamma}}}{P_{Vac}} - 1 \right), \tag{8}$$

where γ is the ratio of specific heats, R is the gas constant, T is the temperature, P_{Dis} is the discharge pressure of the pump (1 bar), P_{Vac} is the average vacuum pressure and η, the pump efficiency, is set to 0.7.[17,18,35,36]

2.4 | Bed working capacity

The working capacity of the adsorbent, n^{ads} is defined here as the maximum change in the quantity of adsorbate (i) that the packed bed can treat in single cycle, and is calculated by the following equation,

$$n_A^{ads} = \sum_i m_{i,ads} \left[Q_{i,A}(p_H, T, y_H) - Q_{i,A}(p_L, T', y'_H) \right], \tag{9}$$

where Q is the methane uptake by adsorbents under the adsorption (p_H, T, y_H) and desorption (p_L, T', y'_H) conditions (Figure S2), respectively.

The bed capacity ratio, $\mathbb{C}$, is a dimensionless quantity introduced by Bhatt et al.[37] and adapted by May and co-workers,[29,38] to quantify the ratio of the adsorbate fed to the bed during a cycle step and the total amount it can store relative to its initial condition. The bed capacity ratio is defined for the cycles considered in this work as:

$$\mathbb{C} = \frac{F \cdot y_F \cdot t_{FE}}{n_A^{gas} + n_A^{ads}}, \tag{10}$$

$$n^{gas} = y_F \times \frac{p_H V_{bed} \varepsilon}{RT}, \tag{11}$$

where n_A^{gas} is the amount of methane that could be added to the gas phase (void space), F is the feed gas flow rate, y_F is the methane

concentration in the feed gas, t_{FE} is the feed gas injection time, p_H is the high pressure of the adsorption step, V_{bed} is the volume of the bed, ε is the void fraction, m_{ads} is the mass of adsorbents. As demonstrated by May and co-workers, $\mathbb{C}$ can be a useful parameter when optimizing the performance of a given cycle and for analyzing the feed flow rate relative to a given adsorbent bed size.

3 | RESULTS AND DISCUSSION

3.1 | Pilot demonstration and process validation

The CH_4/N_2 separation performance was first investigated using the 6-column pilot plant as given in Section 2, with various feed gas concentrations and operational conditions. The detailed operation parameters and results are shown in Table 3. The pilot tests were conducted at an ambient temperature around 18°C which remained within ±3°C during operation. The adsorption and desorption (absolute) pressures were approximately 120 and 22 kPa, respectively. The CH_4 productivity of the cycle increased with higher concentrations of methane in the feed because the higher CH_4 partial pressures increase the amount of adsorption occurring, consistent with the observations recently reported by Hu et al.[32] Trial 2 was an exception and delivered a higher productivity than Trial 3 despite having a lower methane feed concentration because it had a 51% larger feed flow rate, which increased the amount of product generated in the same period of time. However, the larger feed flow also caused breakthrough to occur in the column, which resulted in a higher exhaust concentration (5.0%) and a lower methane recovery (74%).

Figure 3 shows a comparison of the CH_4 concentrations in both the light and heavy streams for the five experimental pilot tests and the corresponding simulations. The CH_4 concentrations of both product streams measured in the pilot demonstrations are consistent with the modeling results, with root mean square deviations (RMSD) below 2 mol%. The comparison further demonstrated the validity of the numerical model on scale. The CH_4 concentration in the light product was always below 5 mol%, and the CH_4 concentration in the heavy product increased proportionally with feed CH_4 concentration. Methane enrichment ratios were between 2.14 and 2.30 when the feed concentration ranged from 5.0% to 16.1%. For CH_4 feed concentrations above 14%, the enriched CH_4 product concentration was above 30%, which is sufficient for use in power generation.[39] It should be noted though, that feed gas impurities such as water, CO_2 and hydrocarbons are commonly present in most sources of natural gas, biogas or coal mine vent streams. These impurities are generally removed to sales gas specifications by various unit operations that would be located upstream of the nitrogen rejection unit. Additionally, to protect the media used to separate N_2 and CH_4 from degradation that may be caused by interactions with such impurities, guard layers of different adsorbents with high affinities for these impurities are often located in the same bed; in this work, the alumina and activated carbon layers served as guard beds for the ILZ. Clearly, the presence and effects of the impurities (while not studied directly in this work) must be taken into consideration while employing ILZ for industrial applications.

Table 4 shows a comparison of the CH_4 enrichment performance achieved in this work with relevant comparable studies on feed gas concentrations below 50% (CH_4%) reported in literature, that uses different adsorbents and/or PSA cycles. The CH_4 enrichment achieved in this study was slightly improved relative to our previous tests with the same material and cycle,[32] which is likely due to the increase in ILZ packing density, that is, 0.66 g/cm^3 for cylindrical ILZ[32] and 0.78 g/cm^3 for the spherical ILZ beads used in this work. The methane enrichment ratio achieved here is 2.2–2.4, which is slightly higher than those reported in the literature using activated carbon or silicate-1 adsorbent.[41,42] The simulation results using novel processes such as

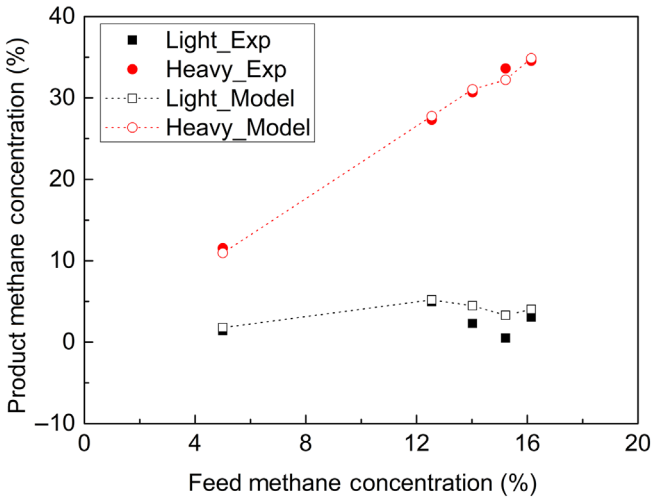

FIGURE 3 A comparison of the experimental and simulation results. Filled symbols denote results from the pilot tests and while hollow symbols connected by the dashed line denote results from the simulation at equivalent conditions

TABLE 3 Operational parameters and results from the pilot demonstration tests

No.	Room temperature, °C	Pressure, kPa.a		Concentration, CH_4%			Feed flow, mol/h	Recovery, CH_4%	Productivity, CH_4 mol/kg/h
		Adsorption	Desorption	Feed	Product	Exhaust			
1	17	118	23	5.0	11.5	1.4	47.0	82	0.013
2	19	119	21	12.5	27.3	5.0	88.9	74	0.057
3	19	117	21	14.0	30.7	2.3	58.8	90	0.051
4	19	117	22	15.2	32.3	0.5	56.0	98	0.058
5	19	122	21	16.1	34.6	3.1	85.8	89	0.084

the concentration thermal swing adsorption and the PSA with simulated moving bed operation mode reported a much higher CH_4 enrichment ratio; these are, however, mostly simulations and/or involve much more complex cycle operations.

3.2 | Process optimization

3.2.1 | Effects of desorption pressure

Desorption is the major step for the regeneration of adsorbents in PVSA cycles. The degree of regeneration determines (i) the working capacity of the adsorbent bed, (ii) the compositions of the product streams, and (iii) the energy consumption of the cycle. The working capacity of the adsorbent bed in this context quantifies the difference between the maximum methane uptake at the end of the adsorption step and the minimum methane uptake at the end of the desorption step, averaged over the bed length.

Figure 4 shows the effects of desorption pressure on the CH_4/N_2 separation performance at constant feed gas concentration, flow rate, and environment temperature. As the desorption pressure decreases, the minimum partial pressure and uptake of CH_4 at that condition also decrease. Hence, the working capacity of the adsorbent bed increases. However, an optimum desorption pressure exists for a given PVSA system. The recovery of CH_4 exceeds 97% when the desorption pressure is 23.5 kPa. Further decreasing the desorption pressure has very little impact on the methane concentration in the light product (0%–1%), or the cycle's methane recovery (97%–100%) and productivity (0.16 mol/cycle/kg), as demonstration in Figure 4A,B.

The concentration of methane in the heavy product drops from 29.1% to 25.0% as desorption pressure decreases from 23.5 to 3 kPa. This is contradictory to overly simplistic expectations that lower desorption pressure will result in higher heavy product concentrations

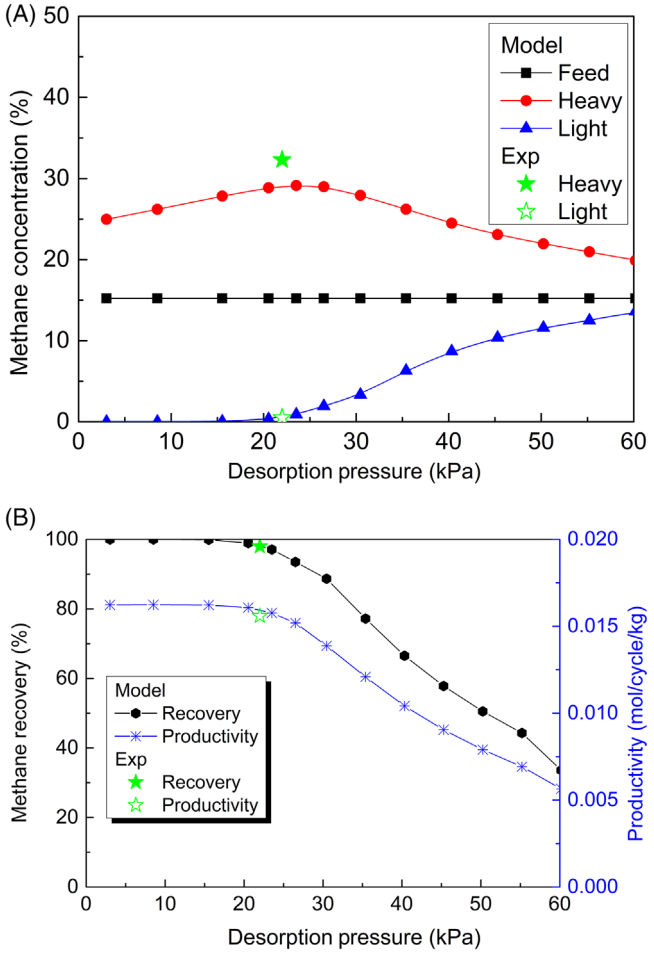

FIGURE 4 Effects of desorption pressure (vacuum) on the performance of CH_4/N_2 separation. The CH_4 concentration in the feed gas and the feed gas flow rate are 15.2% and 56.0 mol/h, respectively. The environment temperature is 20°C

TABLE 4 A comparison of methane enrichment results from this work and literature

No.	Feed CH_4%	Method	Product CH_4%	Recovery CH_4%	Adsorbent	Process	Reference
1	5	Experiment	10	87	ILZ	PSA	32
2	5	Experiment and simulation	12	82	ILZ	PSA	This work
3	5–20	Simulation	99	99	Silicalite	CTSA[a]	40
4	15	Experiment	28	97	ILZ	PSA	32
5	14	Experiment and simulation	31	90	ILZ	PSA	This work
6	17	Experiment	42	~75	AC[b]	PSA	17
7	20	Experiment	40	85	Silicalite-1	PSA	41
8	20	Simulation	40	83	Norit RB1 AC	PSA	42
9	30	Simulation	99	92	AC	PSA-SMB[c]	43
10	44	Experiment	77	98	ILZ	PSA	32
11	50	Simulation	96	99	$[Ni_3(HCOO)_6]$	PSA	35

[a]CTSA, concentration thermal swing adsorption.
[b]AC, activated carbon.
[c]PSA with simulated moving bed operation mode.

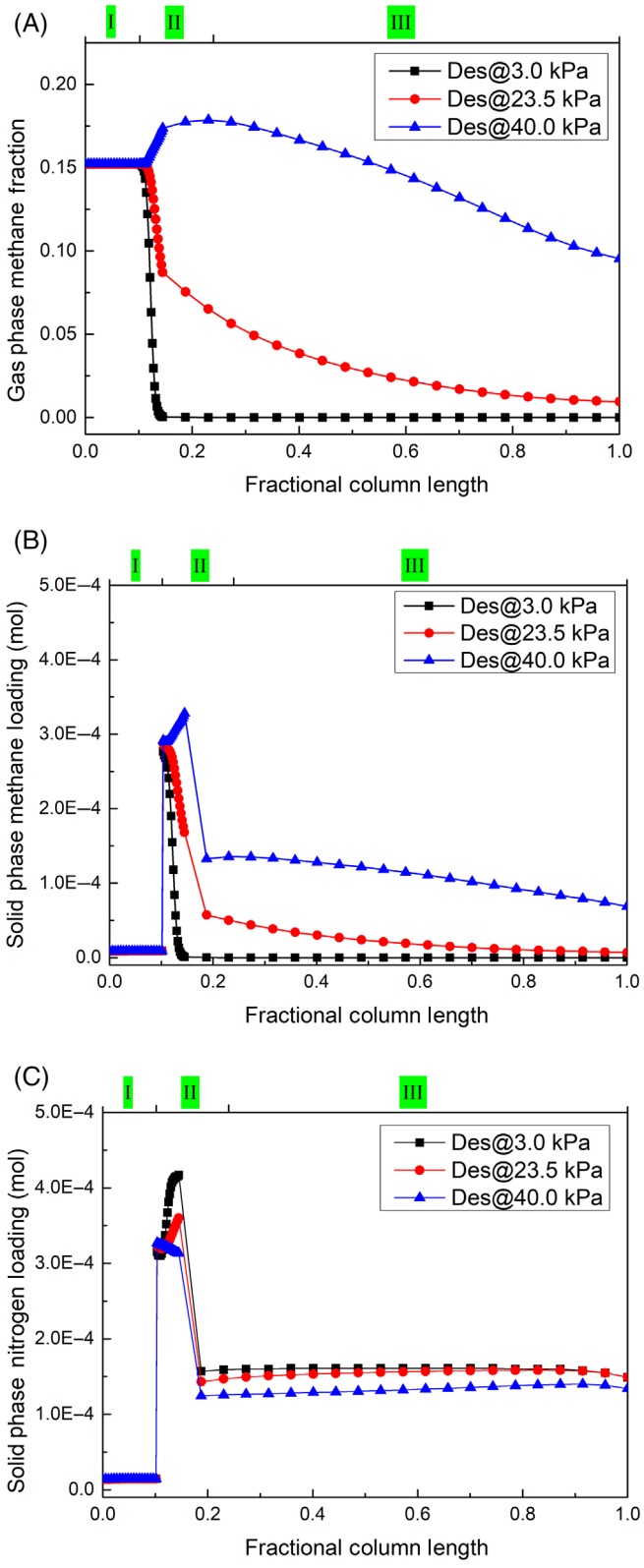

FIGURE 5 Column profiles at the end of the adsorption step (same feed as Figure 4): (A) methane concentration in the gas phase, (B) methane loading on the adsorbents, and (C) nitrogen loading on the adsorbents. The desorption pressures used in the 3 cycles are 3.0, 23.5, and 40.0 kPa, respectively. Layer I, II, and III denotes alumina, activated carbon, and ILZ, respectively

(CH_4) due to a higher driving force. Indeed, the study shown in Figure 4 indicates that the maximum amount of methane desorbed becomes constant at pressures below around 23.5 kPa as methane recovery reaches more than 97%. Rather, the top section of the column uptakes more nitrogen due to insufficient methane supply (Figure 5C), and this nitrogen is evacuated from the column during the desorption step, causing the methane concentration in the heavy product to decline. Therefore, practical operations should aim at optimum desorption pressures, not lower desorption pressures, under operational conditions.

The filled and hollow star symbols represented the results from pilot-scale experiment (No. 4, Table 1). The desorption pressure used in experiment was quite close to the optimum desorption pressure (23.5 kPa) shown in the simulation. The CH_4 concentration in the heavy product from the experiment (filled star symbol in Figure 4A) was slightly higher than the simulated results, while the light CH_4 concentration, CH_4 recovery and productivity were all in good consistency with the simulations.

The decline in heavy product methane concentration when desorption pressures are decreased below 23.5 kPa is related to the extent to which the methane composition front propagates into the bed. Figure 5A–C shows, respectively, the gas phase methane concentration, the adsorbent's methane loading, and its nitrogen loading as a function of axial position in the column at the end of the *adsorption* step for three different desorption pressures. While the bed pressure at the end of the adsorption step is around 120 kPa, the three axial profiles shown correspond to the consequences of having applied different desorption pressures during the cycle.

Three layers containing different adsorbents are present in the bed: a protective bottom layer of alumina at fractional column lengths from 0 to 0.1, a second guard layer of activated carbon at fractional column lengths from 0.1 to 0.24, and the main bed of ILZ at fractional column lengths from 0.24 to 1. The alumina has little effect on the separation given its negligible methane and nitrogen adsorption capacities relative to those of the other layers. However, it does serve as an inert barrier for the gas phase methane front to pass through once the adsorption step begins: for the case of the lowest desorption pressure, the front does not extend past the alumina layer by the end of the adsorption step. Most of the bed is thus not being used to adsorb methane when a desorption pressure of 3 kPa is applied and, instead, the relatively large amount of N_2 adsorbed during the preceding repressurization steps remains loaded on the ILZ. When the vacuum is applied uniformly across the entire extent of the column this N_2 desorbs and the methane concentration in the heavy product declines.

Figure 6 shows that the energy consumption per mole CH_4 produced increased by 166% when the desorption pressure was reduced from 23.5 to 3 kPa. This energy consumption increase reflects the fact that virtually all the methane is recovered into the heavy product stream for a desorption pressure of 23.5 kPa, and that applying a stronger vacuum simply causes work to be done as N_2 is extracted (unnecessarily) into the heavy product stream.

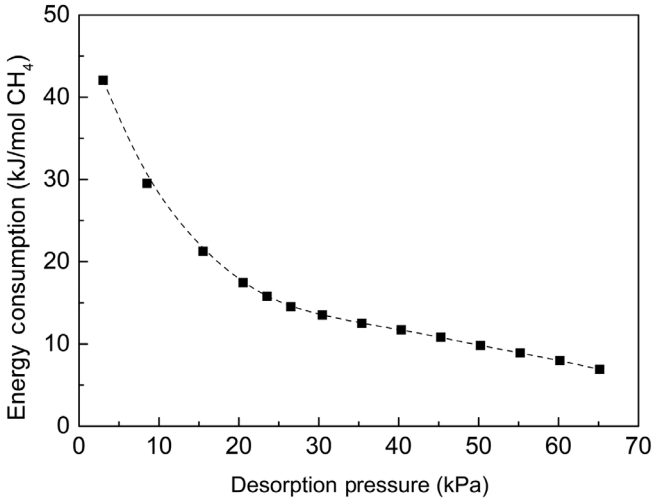

FIGURE 6 Simulated energy consumption (of the vacuum pump) for different desorption pressure conditions at constant feed pressure (120 kPa) and methane concentration (15%)

When the desorption pressure was increased from 30 to 60 kPa, the separation performance also decreased significantly due to the reduced working capacity of the adsorbent bed from 1.0 to 0.5 mol. This is due to the increase in $Q_{i,A}\left(p_L, T', y_H'\right)$ associated with the larger p_L rather than the limited use of the bed's top fraction to adsorb methane. As shown in Figure 4, the result is a decrease in CH_4 recovery and, hence, cycle productivity. This is illustrated by the breakthrough of the gas phase methane front into the top of the adsorption column shown in Figure 5B (Des@40.0 kPa), which results in a large increase of CH_4 concentration in the light product. The heavy product purity also decreases because the N_2 concentration in the gas phase across bed is relatively uniform at the end of the adsorption step; for a desorption pressure of 40 kPa, no distinct front separating the N_2-rich and CH_4-rich zones in the gas phase develops in contrast to the profile observed for a desorption pressure of 23.5 kPa. Consequently, increasing amounts of N_2 breakthrough into the heavy product stream when the desorption pressure is increased. The cycle's energy consumption per mole of methane produced drops from 13 to 8 kJ/mol CH_4 because the loss of methane to the light stream is smaller than the reduction in work associated with changing the desorption from 30 to 60 kPa.

The unexpected observation that lowering the desorption pressure beyond a certain 23.5 kPa leads to a worse separation performance reflects the fact that this modest vacuum produces an optimal methane profile through the bed at the end of the adsorption step. Another cycle parameter that will influence the nature of this gas phase profile is the feed gas flow rate.

3.2.2 | Effects of feed gas flow rate

Figure 7 shows the results of heavy product CH_4 concentration and overall methane recovery as a function of feed flow rates ranging

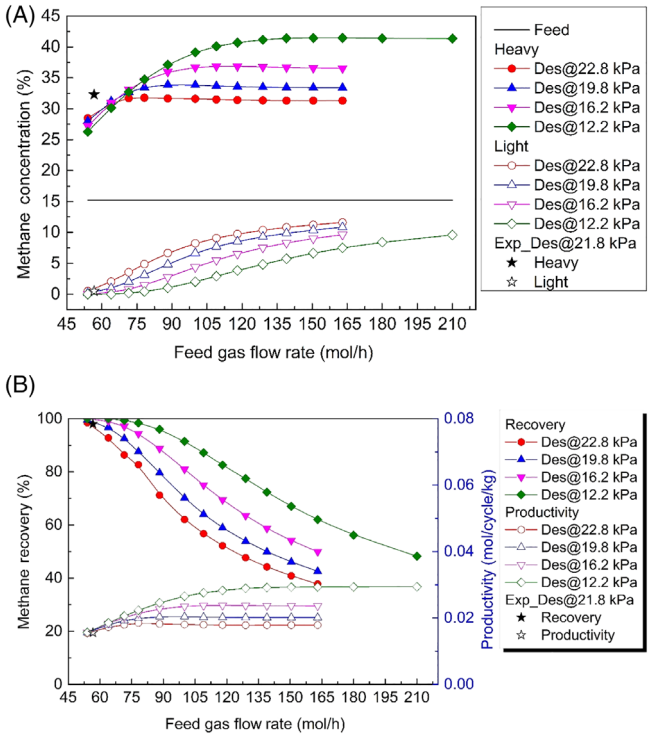

FIGURE 7 Effects of desorption pressure on the performance of the CH_4/N_2 separation for various feed gas flow rates. The methane concentration in the feed gas is 15.2% and the environment temperature is 20°C. In panel (B), the dashed line corresponds to a methane recovery of 80% (see text)

from 50 to 165 mol/h for a range of desorption pressures from 12.2 to 22.8 kPa. At low feed gas flow rates, the recovery of methane is over 99% but the methane concentration in the heavy product is limited. Increasing the feed gas flow results in a proportional rise in heavy product methane concentration, the slope of which depends on desorption pressure, with a corresponding decrease in methane recovery. Eventually, further feed gas injection does not result in any further increase in heavy product purity and then causes a breakthrough of the methane front into the (N_2-rich) waste product, causing further reductions in methane recovery. However, the increase in the amount of feed being means that the cycle's CH_4 productivity remains stable despite the reductions in recovery.

Figure 7 is useful for determining the necessary operational conditions needed to achieve a given separation performance. Taking a methane recovery requirement (80%) as an example, the maximum feed flow rate can be determined for certain desorption pressures (and vice versa) using the dashed line in Figure 7B. A similar approach can also be applied to determine conditions required to achieve a maximum methane product concentration using Figure 7A. The data shown in Figure 8 were extracted from Figure 7A and indicate the feed gas flow rates at which maximum product concentrations are achieved for several different desorption pressures. As desorption pressure increases, both the optimum feed flow rate and the maximum heavy product methane concentration decrease. Methane

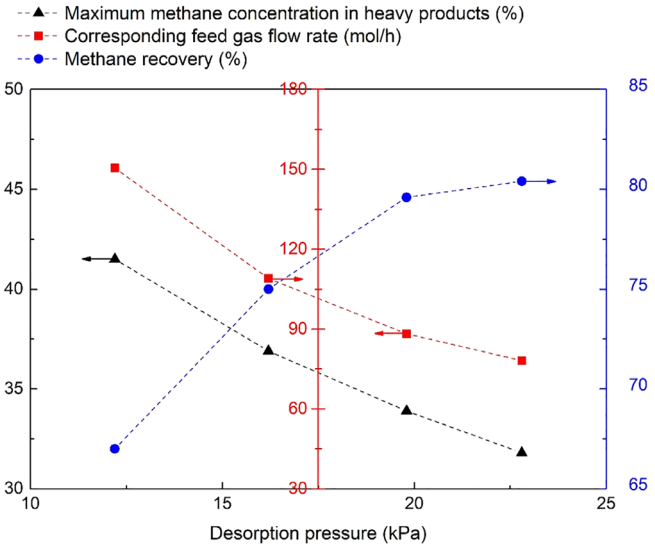

FIGURE 8 The maximum heavy product concentration achieved and corresponding feed flow rates for several different desorption pressures

recovery, however, drops monotonically with decreasing desorption pressure and increasing feed flow.

Figure 9 compares the quantity of the two gas components remaining in the column at the end of the third pressure equalization step PE3 to that at the end of the desorption step for a feed flow rate near the optimum methane recovery condition for a desorption pressure of 22.8 kPa (data shown in Table S1). Two pairs of pressures are compared, with the second pair roughly half of the first. In both cases, the amounts of each component in the void space and adsorbed on the adsorbents are shown. More than 85% of the methane recovered from the column is from the adsorbed phase, that is, $n_A^{ads} = 1.13$ mol and $n_A^{gas} = 0.20$ mol for a desorption pressure of 22.8 kPa, and $n_A^{ads} = 1.43$ mol and $n_A^{gas} = 0.22$ mol for a desorption pressure of 12.2 kPa. The quantity of CH_4 recovered from the solid phase is 61% higher when the desorption pressure is lowered to 12.2 kPa, reflecting the fact that methane recovery increases monotonically with decreasing desorption pressure.

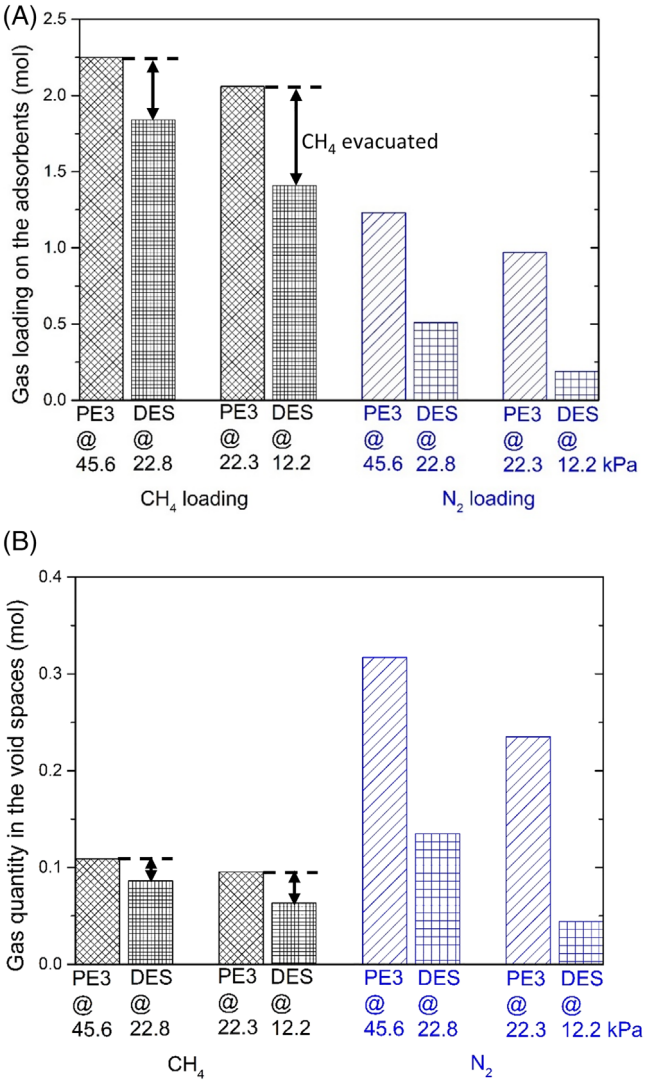

FIGURE 9 Component quantities in the solid (A) and gas (B) phases at the end of the third pressure equalization (PE3) and desorption steps. The methane concentration in the feed gas, feed gas flow rate and environment temperature are 15.2%, 88.2 mol/h, and 20°C, respectively

3.3 | Bed capacity ratio analysis

The bed capacity ratio defined by Equation (10) provides a metric by which the effects of desorption pressure and feed flow rate can be placed on a common basis. Additionally, $\mathbb{C}$ is useful because it provides a general measure of the degree to which the adsorption bed is being utilized that is independent of the column dimensions and feed flow rate. Figure 10 shows how the bed capacity ratio can be used to investigate how the separation performance achieved with PVSA cycles simulated in this work varies with different feed flow rate and desorption pressure.

In Figure 10A, changes in desorption pressure p_L from 12 to 23 kPa are converted to values of $\mathbb{C}$ for three fixed feed flow rates, F, with the resulting methane concentration in the heavy product shown on the vertical axis. The three F values dominate the heavy product purity achieved, with the lowest feed flow generating methane concentrations of 26–29 mol% relative to a feed concentration of 15 mol%, while the highest F produces methane concentrations between 46.2 and 48.6 mol%. This reflects the fact that at the lower feed flow rates, the bed is not being adequately utilized as reflected in the relative values of $\mathbb{C}$: 0.2–0.36 for the lowest flow compared with 0.35–0.44 for the highest. Nevertheless, changing the value of $\mathbb{C}$ values by varying p_L while holding F constant results in the heavy product purity passing through a maximum in all cases. The value of $\mathbb{C}$ at which this optimum occurs increases with feed flow: this result is a generalization of the one shown in Figure 4 and reveals how the more the bed is used the lower the desorption pressure can be before the optimum purity condition is reached.

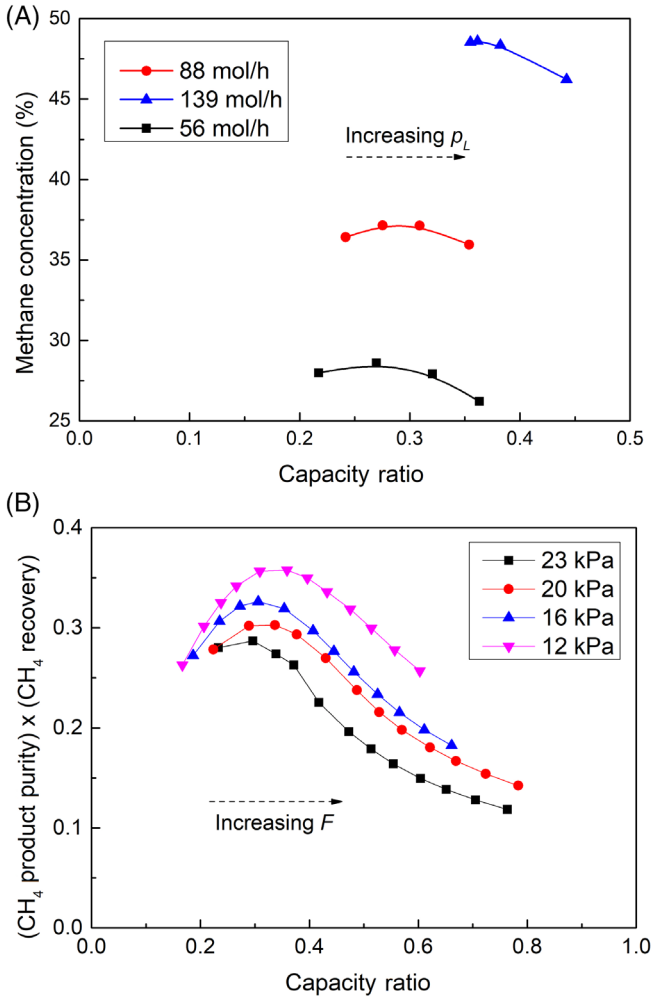

FIGURE 10 Impact of changing the bed capacity ratio $\mathbb{C}$ defined by Equation (10) on two measures of separation performance. (A) Methane concentration in heavy product for three constant feed flow rates, F, for values of $\mathbb{C}$ varied by increasing the desorption pressure, p_L, from 12 to 23 kPa. (B) Product of methane purity and methane recovery at constant p_L for values of $\mathbb{C}$ varied by increasing F from 54 to 163 mol/h

Figure 10B shows the impact of changing feed flow from 54 to 163 mol/h on $\mathbb{C}$ at four fixed values of the desorption pressure. However, if heavy product methane concentration were the only metric of separation performance considered, the figure would look similar to Figure 5A. To go beyond this, Figure 10B captures the inherent trade-off between methane product purity and methane recovery by plotting their product as a function of the bed capacity ratio. The information about the dependence of recovery on F and p_L contained in Figure 5B is combined with that in Figure 5A to produce a set of curves each with a clear maximum for a value of $\mathbb{C}$ in the range 0.29–0.36. This maximum occurs because while using more the bed leads to an increase in purity until an asymptotic limit is reached, it also reads to an increasing loss of methane to the light product with breakthrough of the composition front. Lower desorption pressures produce larger maximum value for the product of purity and recovery because more work per cycle is done.

While product purity and methane recovery are not necessarily of equal value, depending on the context of the particular separation, identifying the value of $\mathbb{C}$ at which their product is a maximum provides a useful starting point for process optimization. The relatively narrow range of optimal $\mathbb{C}$ values for the four values of p_L can be used to infer an appropriate bed volume given a particular feed flow rate. From this starting point, further optimization can be conducted to achieved target values of product purity, methane recovery or cycle duty. Interestingly, optimum values of $\mathbb{C}$ obtained for methane-nitrogen separations of feeds containing either 10 mol%[38] or 40 mol%[29] methane, using either activated carbon or ILZ within a variety of dual-reflux pressure swing adsorption (DR PSA) cycles were usually in the range (0.20–0.30), which is slightly smaller than those found in this work. While $\mathbb{C}$ was calculated using a slightly different formula to account for the use of reflux and a mid-bed feed in the DR PSA cycles, the similarity in the optimum values of $\mathbb{C}$ is noteworthy given the very different sizes of the adsorption columns (0.95 L vs. 35 L) and feed flows (3.3 mol/h vs. 50–160 mol/h).

4 | CONCLUSIONS

The recovery and enrichment of methane from nitrogen were investigated using a new ionic liquidic (ILZ) material and a pressure swing adsorption process with both pilot tests and simulations on the Aspen Adsorption platform. The 6-column PVSA model was able to reliably predict the experimental results with root mean square deviations in the concentrations in the heavy and light streams below 2%. Once the PVSA simulations were validated, further parametric studies explored separation performance and cycle duty as a function of desorption pressure and feed flow rate. Counter-intuitively, decreasing the desorption pressure below a certain threshold led to reductions in heavy product methane purity if the feed flow rate was too small. The bed capacity ratio, $\mathbb{C}$, was shown to provide a useful metric for quantifying utilization of the bed, independent of the particular column dimensions and feed flow rate. Maxima in the combined separation performance metric (methane recovery) $\times$ (methane purity) occurred for values of $\mathbb{C}$ in the range 0.29–0.36 across the four different desorption pressures considered, and are similar to the optimum bed capacity ratios reported for similar methane–nitrogen separations conducted with DR PSA cycles using much smaller columns.

AUTHOR CONTRIBUTIONS

Guoping Hu: Conceptualization (lead), formal analysis (lead), investigation (lead), methodology (lead), resources (lead), software (lead), visualization (lead), writing - original draft (lead), writing - review & editing (lead). **Gongkui Xiao:** Formal analysis (supporting); methodology (supporting); software (supporting); writing – original draft (supporting); writing – review and editing (supporting). **Yalou Guo:** Formal analysis (supporting); software (supporting); writing – review and editing (equal). **Mitch Manning:** Funding acquisition (equal); project administration (equal); resources (supporting); writing – review and editing (supporting). **Li Chen:** Investigation (supporting);

methodology (supporting); resources (supporting); writing – review and editing (supporting). **Lanjin Yu:** Funding acquisition (supporting); investigation (supporting); methodology (supporting); resources (supporting); writing – review and editing (supporting). **Kevin Gang Li:** Conceptualization (supporting); funding acquisition (equal); investigation (supporting); methodology (supporting); supervision (equal); writing – review and editing (supporting). **Eric F. May:** Funding acquisition (equal); investigation (supporting); methodology (supporting); supervision (equal); writing – review and editing (supporting).

ACKNOWLEDGMENTS

The authors acknowledge the support from Global Innovation Linkage (GIL) awarded by Department of Industry, Innovation and Science entitled "Development of Unconventional Gas Technologies for Sustainable Energy Security," the discovery project awarded by Australian Research Council entitled Next Generation Gas Separations via Innovative Adsorption Technologies (DP190100983), and Early Career Researcher Grants Scheme awarded by the University of Melbourne entitled "Production of High Purity Hydrogen from Mixed Pipeline Gases." Special thanks to technicians at DKT Energy Technology Co. Ltd. for their kind assistance in PVSA facilities and plant operation. Open access publishing facilitated by The University of Melbourne, as part of the Wiley - The University of Melbourne agreement via the Council of Australian University Librarians.

CONFLICT OF INTEREST

The authors (Eric F. May, Mitch Manning, Kevin Gang Li) are also Directors of the company Gas Capture Technologies Pty. Ltd. that supplied the ILZ.

DATA AVAILABILITY STATEMENT

Data available on request from the authors.

ORCID

Guoping Hu https://orcid.org/0000-0002-7480-8411
Gongkui Xiao https://orcid.org/0000-0001-9659-6969
Yalou Guo https://orcid.org/0000-0003-4052-9681
Kevin Gang Li https://orcid.org/0000-0003-1700-297X
Eric F. May https://orcid.org/0000-0001-5472-6921

REFERENCES

1. Pachauri RK, Meyer LA. *Climate Change 2014: Synthesis Report*. IPCC; 2014.
2. Buendia EC, Guendehou S, Bundit L, et al. 2019 Refinement to the 2006 IPCC Guidelines for National Greenhouse Gas Inventories. In Gómez D, Irving W, eds. *2019 Refinement to the 2006 IPCC Guidelines for National Greenhouse Gas Inventories*. IPCC Task Force on National Greenhouse Gas Inventories; 2019.
3. Gan Y, El-Houjeiri HM, Badahdah A, et al. Carbon footprint of global natural gas supplies to China. *Nat Commun*. 2020;11(1):824.
4. Initiative GM Coal Mine Methane Country Profiles; 2015. https://www.epa.gov/cmop/coal-mine-methane-country-profiles. Accessed 17 April, 2020.
5. Neininger BG, Kelly BFJ, Hacker JM, Lu X, Schwietzke S. Coal seam gas industry methane emissions in the Surat Basin, Australia: comparing airborne measurements with inventories. *Philos Trans R Soc A Math Phys Eng Sci*. 2021;379:20200458-20200469.
6. Errickson FC, Keller K, Collins WD, Srikrishnan V, Anthoff D. Equity is more important for the social cost of methane than climate uncertainty. *Nature*. 2021;592(7855):564-570.
7. Rufford TE, Smart S, Watson GCY, et al. The removal of CO_2 and N_2 from natural gas: a review of conventional and emerging process technologies. *J Petrol Sci Eng*. 2012;94–95:123-154.
8. Kochunni SK, Chowdhury K. LNG boil-off gas reliquefaction by Brayton refrigeration system—part 1: exergy analysis and design of the basic configuration. *Energy*. 2019;176:753-765.
9. Kurle YM, Wang S, Xu Q. Simulation study on boil-off gas minimization and recovery strategies at LNG exporting terminals. *Appl Energy*. 2015;156:628-642.
10. Lawson S, Al-Naddaf Q, Newport K, Rownaghi A, Rezaei F. Assessment of CO_2/CH_4 separation performance of 3D-printed carbon monoliths in pressure swing adsorption. *Ind Eng Chem Res*. 2021;60:16445-16457.
11. Cavenati S, Grande CA, ArE R. Removal of carbon dioxide from natural gas by vacuum pressure swing adsorption. *Energy Fuel*. 2006;20:2648-2660.
12. Brandani F, Pullumbi P, Monereau C. Nitrogen rejection from landfill gas using pressure swing adsorption. *Adsorption*. 2021;27:603-618.
13. Rasi S, Läntelä J, Rintala J. Upgrading landfill gas using a high pressure water absorption process. *Fuel*. 2014;115:539-545.
14. Yang X, Liu Y-S, Li Y-L, Zhang C-Z, Meng Y, Yang H-J. Low concentration coal mine methane concentrated by vacuum pressure swing adsorption. *2010 International Conference on Digital Manufacturing & Automation*. Vol 1(4); IEEE Computer Society; 2010:896-900.
15. Kim J, Maiti A, Lin LC, Stolaroff JK, Smit B, Aines RD. New materials for methane capture from dilute and medium-concentration sources. *Nat Commun*. 2013;4:1694-1701.
16. Saleman TL, Li G, Rufford TE, et al. Capture of low grade methane from nitrogen gas using dual-reflux pressure swing adsorption. *Chem Eng J*. 2015;281:739-748.
17. Hu G, Zhao Q, Tao L, Xiao P, Webley PA, Li KG. Enrichment of low grade CH_4 from N_2/CH_4 mixtures using vacuum swing adsorption with activated carbon. *Chem Eng Sci*. 2021;229:116152-116163.
18. Qu D, Yang Y, Qian Z, et al. Enrichment of low-grade methane gas from nitrogen mixture by VPSA with CO_2 displacement process: modeling and experiment. *Chem Eng J*. 2020;380:122509-122523.
19. Hosseini SS, Chung TS. Carbon membranes from blends of PBI and polyimides for N_2/CH_4 and CO_2/CH_4 separation and hydrogen purification. *J Membr Sci*. 2009;328:174-185.
20. Kapoor R, Ghosh P, Kumar M, Vijay VK. Evaluation of biogas upgrading technologies and future perspectives: a review. *Environ Sci Pollut Res*. 2019;26:11631-11661.
21. Yang Z, Wang D, Meng Z, Li Y. Adsorption separation of CH_4/N_2 on modified coal-based carbon molecular sieve. *Sep Purif Technol*. 2019;218:130-137.
22. Kim M-B, Bae Y-S, Choi D-K, Lee C-H. Kinetic separation of landfill gas by a two-bed pressure swing adsorption process packed with carbon molecular sieve: nonisothermal operation. *Ind Eng Chem Res*. 2006;45:5050-5058.
23. Weh R, Xiao G, Islam MA, May EF. Nitrogen rejection by dual reflux pressure swing adsorption using Engelhard Titanosilicate Type 4. *Ind Eng Chem Res*. 2021;59:22573-22581.
24. Majumdar B, Bhadra SJ, Marathe RP, Farooq S. Adsorption and diffusion of methane and nitrogen in barium exchanged ETS-4. *Ind Eng Chem Res*. 2011;50:3021-3034.
25. Gu M, Zhang B, Qi Z, et al. Effects of pore structure of granular activated carbons on CH_4 enrichment from CH_4/N_2 by vacuum pressure swing adsorption. *Sep Purif Technol*. 2015;146:213-218.
26. Rufford TE, Watson GCY, Saleman TL, Hofman PS, Jensen NK, May EF. Adsorption equilibria and kinetics of methane + nitrogen

mixtures on the activated carbon Norit RB3. *Ind Eng Chem Res*. 2013; 52:14270-14282.
27. Zhang J, Liu H, Zhou F, Li X, Wei K, Song J. Enrichment of oxygen-containing low-concentration coalbed methane with CMS-3KT as the adsorbent. *ACS Omega*. 2021;6:6914-6923.
28. Li G, May EF, Webley PA, Huang SH-W, Chan KI, Inventors. Method for gas separation. US patent 10562005B22017.
29. Weh R, Xiao G, Ashraful Islam M, May EF. Upgrading sub-quality natural gas by dual reflux-pressure swing adsorption using activated carbon and ionic liquidic zeolite. *Chem Eng J*. 2020;392:123753-123762.
30. Weh R, Xiao G, Islam MA, May EF. Nitrogen rejection from natural gas by dual reflux-pressure swing adsorption using activated carbon and ionic liquidic zeolite. *Sep Purif Technol*. 2020;235:116215.
31. Saleman TLH. *Adsorption-Based Separations of Gaseous Nitrogen and Methane Mixtures*. School of Mechanical and Chemical Engineering, The University of Western Australia; 2016.
32. Hu G, Zhao Q, Manning M, et al. Pilot scale assessment of methane capture from low concentration sources to town gas specification by pressure vacuum swing adsorption (PVSA). *Chem Eng J*. 2022;427: 130810-130816.
33. Zhang Y, Saleman TLH, Li G, Xiao G, Young BR, May EF. Non-isothermal numerical simulations of dual reflux pressure swing adsorption cycles for separating N_2+CH_4. *Chem Eng J*. 2016;292:366-382.
34. Kubicek M, Hlavacek V. *Numerical Solution of Nonlinear Boundary Value Problems With Applications*. Courier Corporation; 2008.
35. Águeda Maté VI, Delgado Dobladez JA, Álvarez-Torrellas S, Larriba M, Martínez RÁ. Modeling and simulation of the efficient separation of methane/nitrogen mixtures with [$Ni_3(HCOO)_6$] MOF by PSA. *Chem Eng J*. 2019;361:1007-1019.
36. Erden L, Ebner AD, Ritter JA. Separation of landfill gas CH_4 from N_2 using pressure vacuum swing adsorption cycles with heavy reflux. *Energy Fuels*. 2018;32:3488-3499.
37. Bhatt TS, Storti G, Rota R. Optimal design of dual-reflux pressure swing adsorption units via equilibrium theory. *Chem Eng Sci*. 2013; 102:42-55.
38. May EF, Zhang Y, Saleman TL, Xiao G, Li GK, Young BR. Demonstration and optimisation of the four dual-reflux pressure swing adsorption configurations. *Sep Purif Technol*. 2017;177:161-175.
39. Karakurt I, Aydin G, Aydiner K. Mine ventilation air methane as a sustainable energy source. *Renew Sustain Energy Rev*. 2011;15:1042-1050.
40. Delgado JA, Águeda VI, García J, Álvarez-Torrellas S. Simulation of the recovery of methane from low-concentration methane/nitrogen mixtures by concentration temperature swing adsorption. *Sep Purif Technol*. 2019;209:550-560.
41. Yang J, Bai H, Shang H, Wang J, Li J, Deng S. Experimental and simulation study on efficient CH_4/N_2 separation by pressure swing adsorption on silicalite-1 pellets. *Chem Eng J*. 2020;388:124222-124231.
42. Karimi K, Fatemi S. Methane capture and nitrogen purification from a nitrogen rich reservoir by pressure swing adsorption; experimental and simulation study. *J Environ Chem Eng*. 2021;9:106210-106224.
43. Qian Z, Yang Y, Li P, Wang J, Rodrigues AE. An improved vacuum pressure swing adsorption process with the simulated moving bed operation mode for CH_4/N_2 separation to produce high-purity methane. *Chem Eng J*. 2021;419:129657-129671.

SUPPORTING INFORMATION

Additional supporting information may be found in the online version of the article at the publisher's website.

How to cite this article: Hu G, Xiao G, Guo Y, et al. Separation of methane and nitrogen using ionic liquidic zeolites by pressure vacuum swing adsorption. *AIChE J*. 2022;e17668. doi:10.1002/aic.17668